Materials Today Communications 38 (2024) 108120

Contents lists available at ScienceDirect

Materials Today Communications

journal homepage: www.elsevier.com/locate/mtcomm

Combined experimental and theoretical investigation on the structural, electronic, magnetic and optical properties of Pr_2CoFeO_6 double perovskite

M. Dhilip [a,*], Sundaramurthy Rameshkumar [b], Ramesh Kumar Raji [c], Tholkappiyan Ramachandran [d,e], J. Stella Punitha [f], F. Regan Maria Sundar Raj [g], K. Saravana Kumar [h], V. Anbarasu [i], Nandakumar Sekar [j], Rajivganthi Chinnathambi [k], Ayman A. Ghfar [l]

[a] *Microwave Tube Research and Development Centre, Defence Research and Development Organisation, Ministry of Defence, Jalahalli, Bengaluru, Karnataka 500 013, India*
[b] *Department of Physics, Sri Indu College of Engineering and Technology (Autonomous), Hyderabad, Telangana 501 510, India*
[c] *Department of Physics, Surana College (Autonomous), Bengaluru, Karnataka 560 004, India*
[d] *Department of Physics, College of Science, United Arab Emirates University, P.O. Box. 15551, Al-Ain, United Arab Emirates*
[e] *Department of Physics, Saveetha School of Engineering, Saveetha Institute of Medical and Technical Science, Chennai 602105, India*
[f] *Department of Physics, SRM Institute of Science and Technology, Ramapuram Campus, Chennai, Tamil Nadu 600 089, India*
[g] *Department of Physics, Jeppiaar Engineering College, Chennai 600119, Tamil Nadu, India*
[h] *Department of Physics, Sri S. Ramasamy Naidu Memorial College, Sattur, Tamil Nadu 626 203, India*
[i] *Department of Physics (Self-Finance), PSG College of Arts & Science (Autonomous), Coimbatore, Tamil Nadu 641 014, India*
[j] *Department of Physics, Arignar Anna Government Arts College for Women, Walajapet, Tamil Nadu 632 513, India*
[k] *Division of Mathematics, School of Advanced Sciences, Vellore Institute of Technology, Chennai, Tamil Nadu 600 127, India*
[l] *Department of Chemistry, College of Science, King Saud University, P.O. Box 2455, Riyadh 11451, Saudi Arabia*

ARTICLE INFO

Keywords:
Pr_2CoFeO_6
Structural property
Electronics property
Photoluminescence
Dielectric property
Magnetic property

ABSTRACT

The praseodymium-based double perovskite compound with the composition of Pr_2CoFeO_6 has been reported for the very first time. The solid-state reaction technique was used for the synthesis of the Pr_2CoFeO_6 compound. The structural, magnetic, vibrational, dielectric, and luminescent properties of Pr_2CoFeO_6 double perovskite have been investigated by X-ray diffraction, Ultraviolet-visible (UV-Vis) spectrophotometer, photoluminescence, vibrating-sample magnetometer, Raman spectroscopy, and density functional theory calculations. From the X-ray analysis, it is noticed that the compound crystallizes in orthorhombic structure within the *Pbnm* space group. It is also noted that the calculated lattice constant and Wyckoff position values are in good agreement with the experimental results. X-ray photoelectron spectroscopy validated the valence states of Pr, Co, and Fe, revealing the presence of Pr^{3+} and Pr^{4+}, Co^{2+} and Co^{3+}, as well as Fe^{3+} and Fe^{4+}. The semiconducting nature of the prepared compound was identified with UV-Vis analysis and the obtained energy gap value of 2.73 eV is also quite consistent with the theoretical predictions. The Photoluminescence spectrum revealed two emissions (blue-green) caused by transitions of $^3P_0 \rightarrow {}^3H_4$, $^3P_0 \rightarrow {}^3H_5$, and $^3P_0 \rightarrow {}^3H_6$, which are mostly due to the contribution of Pr^{3+} ions. The dielectric property is characterized by varying frequencies in the range from 1 kHz to 1 MHz when the temperature changes from 423 to 563 K. We demonstrate, for the first time, that the magnetic properties are ferromagnetic. The magnetization behavior of the title compounds exhibits the ferromagnetic nature. The M–T curve at 2k Oe for Pr_2CoFeO_6 indicates a decline in magnetization with increasing temperature, revealing a Curie temperature at 562 K, signifying the loss of ferromagnetic property due to FM-AFM ordering interplay. With the tailored properties, therefore, this compound is a potential candidate for application in data storage devices and light-emitting diodes.

* Corresponding author.
E-mail addresses: ceramatdhilip@gmail.com (M. Dhilip), srameshkumarg@gmail.com (S. Rameshkumar).

https://doi.org/10.1016/j.mtcomm.2024.108120
Received 24 August 2023; Received in revised form 10 January 2024; Accepted 12 January 2024
Available online 16 January 2024

1. Introduction

Perovskite (ABO_3) materials have advantages for new functional materials and accommodate a wide range of element substitutions [1]. These materials reveal interesting magneto-resistance [2], superconductivity [3], and ferroelectricity [4]. At present, double perovskite materials based on transition metals attract peculiar attention [5–10], in particular Bi_2FeMnO_6 [11], La_2FeMnO_6 [12] and La_2NiMnO_6 [13], because of their magneto-electric properties. The praseodymium cobalt oxide-based materials have attracted much attention for catalysis and LED applications [14]. Recently a few research works have been carried out on praseodymium with transition metal oxide double perovskite [15–19] for multifunctional applications. Nibedita Das et al. [15] reported that the Pr_2FeCrO_6 compound was found orthorhombic structure, ferromagnetic nature at room temperature and magnetic transitions occur under the below 250 K. Zhongqi Dong and Suhua Yin et al. [16] investigated the crystal structure, microstructure, and magnetic behavior of the RE_2FeCoO_6 (RE = Er and Gd) compounds. They reported that these compounds possess a single-phase structure and Gd_2FeCoO_6 compound considerable for cryogenic magnetic refrigeration. G. R. Haripriya et al. [17] investigated the temperature-dependent structural studies on A_2FeCoO_6 (A= Dy, Eu, Sm, and Ho) compounds, Dy_2FeCoO_6 and Ho_2FeCoO_6 exhibited mixed phases of orthorhombic with monoclinic, but Sm_2FeCoO_6 and Eu_2FeCoO_6 compounds exist as single phases with orthorhombic structure. Moumita Das and Prabhat Mandal [18] have investigated the magneto-dielectric, magneto-caloric, and magnetic properties of the Ho_2FeCoO_6 compound. They have observed spin reorientation transitions at ~45 K and Neel temperature at ~ 270 K. Under the applied magnetic field, they identified the high non-linear difference of the dielectric constant at low temperatures. G. R. Haripriya et al. [19] investigated the ordering of magnetic phase transitions of Sm_2FeCoO_6 and Dy_2FeCoO_6 compounds. They reported that the disordered double perovskites of these compounds exhibit spin re-orientation at ~86 K and magnetic transition found at ~210 K. These both (Sm_2FeCoO_6 and Dy_2FeCoO_6) compounds exhibited first-order spin re-orientation. The electronic and structural properties of Pr_2CoFeO_6 have been investigated by XPS, Raman, and XAS spectrum analysis at 300 K [20]. It is reported that the Co and Fe ions exhibit + 3 oxidation states, which are turning to form the B-site disordered of this compound. Further XPS spectra identified that Pr ions yielded the trivalent valence states and not presented electronic states at the Fermi level. HaoWu et al. [21] reported Pr_2CoFeO_6 to have non-toxic, low cost, excellent thermal stability, and thermoelectric properties. It is an interesting and significantly expanded research for industrial application. This compound exhibits a narrow band gap with a p-type semiconductor. Based on the literature, there is no reported solid-state reaction technique utilizing Pr_2CoFeO_6 preparation and a combination of experimental and theoretical results of structural, electronic, and magnetic properties, dielectric, and luminescence behavior. It has motivated us to investigate structural, Raman, luminescence, magnetic, dielectric, and electronic properties of the Pr_2CoFeO_6 compound by combining experimental and theoretical methods. In the present work, we have the synthesis and characterization of X-ray diffraction, UV–vis, photoluminescence, and Raman spectroscopy of the Pr_2CoFeO_6 compound.

2. Synthesis and characterization

2.1. Preparation of Pr_2CoFeO_6

Pr_6O_{11}, Co_3O_4, and Fe_2O_3 were used as starting materials to make the bulk Pr_2CoFeO_6 material. The mixture of starting ingredients was first pre-calcined at 900 °C in the air. The motivation of the pre-calcined temperature is to easily remove the impurities from the pristine material. The oxides were then blended, and crushed and stoichiometries ratios were placed in an alumina crucible. To get a homogenous mixture, the mixture was heated several cycles in the air at 1000 °C and 1200 °C with different intermediate grind steps and then collected samples.

2.2. Characterizations

Using the X-ray diffraction technique, the crystal structure of the prepared Pr_2CoFeO_6 compound has been analyzed and Rietveld refinement has been performed by FULLPROF software [22]. For the examination of morphology, the Bruker Scanning Electron Microscopy (SEM) apparatus was used to produce the emission scanning electron micrographs and Energy Dispersive X-ray (EDX) analysis data. The UV absorption spectrum (Shimadzu UV-2600i with ISR-2600 plus UV–VIS–NIR spectrophotometer) has been used to analyze the absorption behavior. The Raman spectrum has been taken by the Mono Vista CRS+ Raman microscope system with excitation wavelength 532. The oxidational compositions and chemical valence states of the examined samples were analyzed using X-ray photoelectron spectrometry (XPS) with an ESCALAB 220i-XL instrument manufactured by VG Scientific. The photoluminescence (PL) spectrum was measured by Omni Chrome, Model 532-MAP USA with an Argon ion laser. The magnetic properties have been studied in the Lakeshore VSM 7410 S instrument. The dielectric measurements have been carried out by N4L PSM1735 Numetriq (Phase sensitive multimeter) – LCR Active Head (N4L) in the frequency from 10 Hz to 1 MHz.

2.3. Computational method

The electronic structure calculation of the Pr_2CoFeO_6 has been investigated by the Vienna Ab initio Simulation Package [23]. The Generalised Gradient Approximation (GGA) has been used for the PBE exchange-correlation function [24]. The electronic configurations explicitly used in the computations were as follows: Pr_3 – [Xe] 6 s^2 4 f^3; Co_sv – 3d^8 4 s^1; Fe_sv – 3d^7 4 s^1; O – 2 s^2 2p^4. The symbol _sv represented s electrons, which treated semi-core s states as valence electrons. The symbol _3 indicates valence electron, most of the rare earth compounds adopt a valence state 3, and the remaining f electrons are placed in the core. An interaction between core and valence electrons is treated by a projector augmented wave method (PAW) [25] and electronic wave functions are expanded with the cut-off energy 650 eV. The 6 × 4 × 6 k-point mesh was selected for the Monkhorst-Pack scheme [26]. The total energy was set to be less than 10^{-6} eV/atom for self-consistent convergence and the highest force on the atom was set to be less than 0.01 (eV/Å). The volume and atomic coordinates are fully optimized. For the ferromagnetic calculations, we have selected spin-polarised options. The GGA+*U* coulomb corrections have been used to calculate the electronic density of states. The transition metals and rare earth elements are strongly correlated *d* electrons, it is required to improve descriptions instead of GGA. This correction is solved by DFT+U [27, 28]. In general, DFT energy functional approximations (LDA and GGA) are corrected by additional terms of effective onsite electron-electron interaction using the Hubbard model (U) [29,30]. This is one of the common methods to determine the appropriate U value to compare the band gap for the set of U values with the experimental band gap. Thus, we find the suitable U parameter for the Pr, Co, and Fe atoms by increasing the U parameter. Within the GGA+*U* approach, the band gap increases with the increase of the U parameter, confirming the fact that a Hubbard-like correction term (U) substantially improves the accuracy of the calculated band gap. Finally, the obtained accurate gap with U = 14 eV, which is 90% agreement with our experimental results.

3. Results and discussion

3.1. Structural property

The structural properties of the Pr_2CoFeO_6 sample have been analyzed by powder X-ray diffraction (XRD) data and fitted with Rietveld refinement using FULLPROF software. The XRD and Rietveld

refinement data are presented in Fig. 1. This figure shows that the sharp peaks in the XRD result concluded that the compound exhibited a single phase of orthorhombic structure with the Pbnm space group. Further, electronic structure calculation has been performed in ferromagnetic ordering spin polarised calculations. The experimental and simulated lattice constant and atomic coordinates are presented in Table 1.

It shows that both results are a good match with each other. The Wyckoff position of this structure observed that Pr and O1 atoms occupy in 4c sites, Fe/Co atoms are located at the 4a site and the O2 atom occupies in 8d position [31]. Its crystal structure is presented in Fig. 2. The Goldschmidt tolerance factor (T_f) [32] is used to identify the structural stability along with the tendency for structural deformation, which can be predicted by the following relation,

$$T_f = \frac{R_{Pr} + R_O}{\sqrt{2}[\frac{R_{Co}+R_{Fe}}{2} + R_O]} \quad (1)$$

Where, R_{Pr}, R_{Co}, $R_{Fe,}$ and R_O represent ionic radii of Pr, Co, Fe, and O ions [33] respectively. The calculated Tf value was observed to be 0.90, attributed to the influence of varying ionic radii of Co and Fe ions as indicated by the XPS data [34]. Further, the width of the XRD peaks is directly related to the size of the crystalline nature. The broadened and strong nature of the XRD pattern concluded crystalline behavior. Its crystallite size has been calculated by the Debye-Scherrer relations as,

$$D = 0{\cdot}94\lambda/\beta \cos\theta \quad (2)$$

Where D represents the average crystallite size, λ stands for the CuKα radiation wavelength, β stands for full-width half maximum (FWHM) and θ represents the Bragg angle. The estimated average crystallite size is 52 nm. Our synthesized Pr_2CoFeO_6 double perovskite exhibited single-phase orthorhombic (Pnma) with a disordered structure as confirmed by X-ray diffraction spectroscopy. Due to the disordered orthorhombic structured Pr_2CoFeO_6 compound turning the + 3 valence state at B-site (Co and Fe) ions, which is confirmed by Pal Arkadeb et al. [20] result. It is suggested that they investigated the Pr_2CoFeO_6 compounds by XRD, Raman spectroscopy, XPS, and XAS spectra and compared the results with theoretical ones.

3.2. Morphological analysis

The morphology of the Pr_2CoFeO_6 compound has been analyzed by Scanning electron microscopy (SEM). The Energy Dispersive X-ray (EDX) is used to identify the presence of each element. The SEM image and EDX spectrum of the Pr_2CoFeO_6 are presented in Fig. 3. The SEM image depicts that agglomerated tiny particles are uneven in shape and size. The aggregation of the particles is attributed to the solid-state reaction at very high temperatures [35]. The EDX data is presented in Table 2, it reveals that these chemical compositions are near to the nominal one and it is very close to the stoichiometry of Pr_2CoFeO_6. The EDX data further confirm the successive synthesis of the Pr_2CoFeO_6.

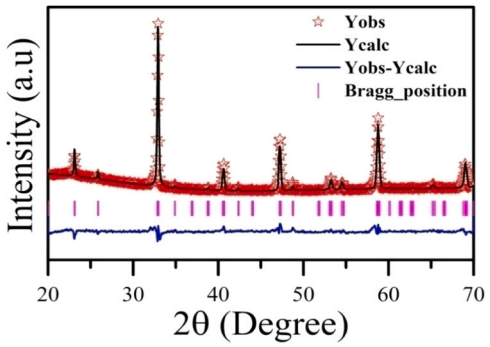

Fig. 1. Rietveld Refinement of the Pr_2CoFeO_6 compound.

3.3. Raman spectroscopy

The vibration properties of the Pr_2CoFeO_6 compound have been characterized by Raman Spectroscopy as presented in Fig. 4. From this Raman spectrum, it shows that the peaks are observed at 637 cm^{-1}, which exhibits a strong phonon and corresponds to the octahedral symmetrical stretching of BO_6. The peak at 640 cm^{-1} is assigned to the asymmetric stretching, vibration in BO_6 octahedral. At a wavelength range of 524 cm^{-1} assigned as bending and anti-stretching. An octahedral bending appears at 414 cm^{-1}, which is due to the Pr^{3+} ion movement of the x and z plane and outer phase tilt along the x-axes with Pr^{3+} and apical O^{2-} move in x and z planes respectively. A single mode at a high region (1261 cm^{-1}) is presented, which corresponds to a combination of bending, symmetrical stretching, and symmetrical stretching overtone. There are lots of difficulties in lack of intensity bands, overlapping of the bands, and instrumental poor resolutions observing all the expected modes in polycrystalline samples. Since experimentally we have achieved six first and second orders Raman modes, it is strong evidence that Pr_2CoFeO_6 belongs to the orthorhombic *Pbnm* symmetry. Further group theory analysis has been performed in this compound, and it shows that Pr_2CoFeO_6 confirmed orthorhombic structure with *Pbnm* space group, its point group is $D_{2\,h}$ and total and projected irreducible representations are given in Table 3. The Pr_2CoFeO_6 compound has 10 atoms per molecular formula and its unit cell is Z = 2, which means 20 atoms are presented per unit cell. Each atom has three degrees of freedom. Totally obtained 60 numbers of irreducible representations as given below,

$$\Gamma_{total} = 7A_g + 8A_u + 5B_{1\,g} + 10B_{1\,u} + 7B_{2\,g} + 8B_{2\,u} + 5B_{3\,g} + 10B_{3\,u}$$

The total numbers of modes (60) are further divided into two groups acoustic (3) modes and optic modes (57) as given below,

$$\Gamma_{acoustic} = B_{1\,u} + B_{2\,u} + B_{3\,u} \text{ and}$$

$$\Gamma_{optic} = 7A_g + 8A_u + 5B_{1\,g} + 9B_{1\,u} + 7B_{2\,g} + 7B_{2\,u} + 5B_{3\,g} + 9B_{3\,u}$$

Finally, it exhibited 24 Raman-active modes ($7A_g + 5B_{1\,g} + 7B_{2\,g} + 5B_{3\,g}$) and 25 IR modes ($9B_{1\,u} + 7B_{2\,u} + 9B_{3\,u}$).

3.4. X-ray photoelectron spectroscopy

The Pr_2CoFeO_6 compound underwent analysis of its elemental composition and valence state through an XPS study, with the findings depicted in Fig. 5. The wide-spectrum confirmation of elements such as Pr, Co, Fe, and O in the compound indicates the absence of any additional or impurity phases. From Fig. 5b, Examining the Pr 3d spectrum in XPS revealed two peaks at approximately 930 eV for Pr $3d_{3/2}$ and 959 eV for Pr $3d_{5/2}$ in the Pr_2CoFeO_6 compound, aligning closely with literature values [32]. Deconvolution of the Pr $3d_{5/2}$ peak disclosed two sub-peaks at 930.2 eV and 959.6 eV, corresponding to the presence of Pr^{3+} and Pr^{4+} ions in the compound [11]. The oxidation state of Co in the Pr_2CoFeO_6 compound was deduced from the high-resolution Co 2p spectra. Fig. 5c illustrates the fitted XPS spectra, showing spin–orbit components, Co $2p_{3/2}$, and Co $2p_{1/2}$, at binding energy values of 781 eV and 796 eV. Deconvolution of the Co $2p_{3/2}$ peak in the Pr_2CoFeO_6 compound revealed two peaks at 774.5 eV and 782.5 eV, indicating the coexistence of Co^{2+} and Co^{3+} ions [10]. Additional satellite peaks at 786.6 and 804.3 eV were identified. The ratio of Co^{2+}:Co^{3+} in the Pr_2CoFeO_6 compound is determined to be 79:21 by using these deconvoluted peak areas. Fig. 5d displays XPS Fe 2p core level spectra for the Pr_2CoFeO_6 compound. According to the spin-orbit coupling rule, the Fe 2p core level exhibited doublet peaks for Fe $2p_{3/2}$ and Fe $2p_{1/2}$ at binding energies of approximately 711 and 725 eV, respectively. An additional satellite peak was observed at around 719 eV in the Pr_2CoFeO_6 compound. Deconvolution of the Fe $2p_{3/2}$ peak revealed two sub-peaks at approximately 709.4 eV and 711.4 eV, indicating Fe^{3+} and

Table 1
The lattice constant and Wyckoff position of the Pr_2CoFeO_6 compound.

Lattice constant (Å)			R_p	R_{wp}	R_{exp}	χ^2	Wyckoff position			
A	b	c						x	y	z
5.439[(a)]	7.688[(a)]	5.456[(a)]	33.8	18.5	8.24	5.04	Pr (4c)	0.4696[(a)]	0.25[(a)]	0.00[(a)]
5.435[(b)]	7.703[(b)]	5.488[(b)]						0.4581[b]	0.2436[(b)]	0.9910[(b)]
							Co/Fe (4a)	0.00[(a,b)]	0.00[(a,b)]	0.00[(a,b)]
							O1 (4c)	0.0755[(a)]	0.25[(a)]	0.0604[(a)]
								0.0089[(b)]	0.2459[(b)]	0.0687[(b)]
							O2 (8d)	0.2780[a]	0.9510[a]	0.2174[(a)]
								0.2876[(b)]	0.9602[(b)]	0.2119[(b)]

[(a)] Present experimental work,
[(b)] present theoretical work

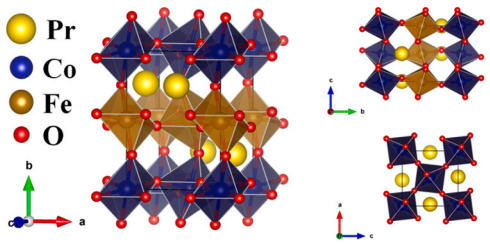

Fig. 2. The crystal structure of the Pr_2CoFeO_6 compound.

Fe^{4+} oxidation states in the Pr_2CoFeO_6 compound [35]. Using these deconvoluted peak areas, the ratio of Fe^{3+}:Fe^{4+} in the Pr_2CoFeO_6 compound is found to be 77:33. Fig. 5e illustrates the O 1 s XPS peak of the Pr_2CoFeO_6 compound, with the spectra fitting well into a single peak at 531.57 eV. The 531.57 eV binding energy is referred to as a shoulder peak, arising from chemisorbed oxygen species on the sample surface [10].

3.5. Optical, electronic and magnetic properties

The absorption behavior of the Pr_2CoFeO_6 compound has been investigated by UV–vis absorption spectroscopy from 220–1000 nm ranges presented in Fig. 6. It shows that absorption peaks are detected at 246 and 370 nm. These peaks are due to the band transition from the valence band (O_{2p}) to the conduction band (Fe_{3d}). The optical band gap (E_g) has been estimated by Tauc's relation [36],

$$(\alpha E_p) = C\,(E_p - E_g)^m \quad (3)$$

Where E_p ($E_p = hv$) denotes the incident photon energy, C denotes the probability of the transition constant, and m specifies the optical absorption transition nature. As shown in Fig. 6, the calculated band gap of the prepared samples is 2.73 eV. It depicts that this material exhibits a semiconductor nature.

The electronic behavior of Pr_2CoFeO_6 compounds with Ferromagnetic (FM) ordering was carried out theoretically. The calculated spin polarised total and projected density of states of electron and charge density contour are presented in Fig. 7. The band gap value is equal to 2.3 eV which is in agreement with our experimental measurements.

Table 2
EDX data of the Pr_2CoFeO_6 compound.

Element	Mass Norm. (%)	Atom (%)
Pr	49.67	12.81
O	33.72	76.61
Fe	9.63	6.27
Co	6.99	4.31
Total	100	100

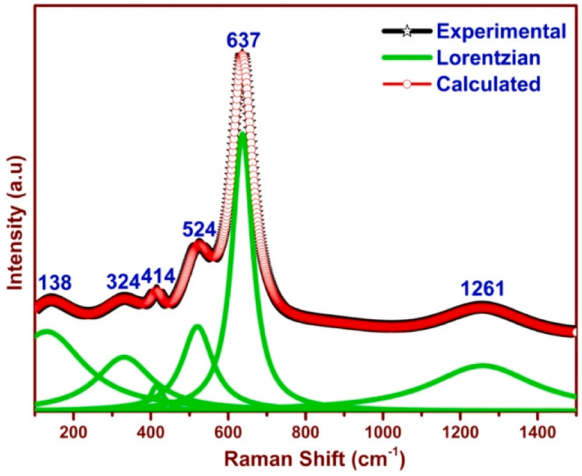

Fig. 4. Raman-active region of the Pr_2CoFeO_6 compound.

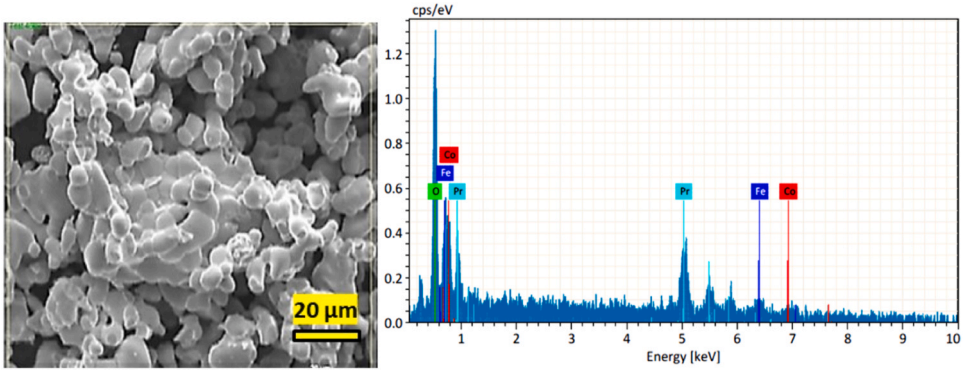

Fig. 3. SEM image with 20 µm field of view and EDX pattern of the Pr_2CoFeO_6 compound.

Table 3
Each atomic contribution of an irreducible representation, site symmetry, Raman, and IR active modes of the Pr_2CoFeO_6 compound.

Atom	Wyckoff sites	Symmetry	Irreducible representations	Raman active	IR active
Sr	4c	C_s	$2A_g + A_u + B_{1\,g} + 2B_{1\,u} + 2B_{2\,g} + 2B_{2\,u} + B_{3\,g} + 2B_{3\,u}$	A_g, $B_{1\,g}$, $B_{2\,g}$, $B_{3\,g}$	$B_{1\,u}$, $B_{2\,u}$, $B_{3\,u}$
Co(Fe)	4b	C_i	$3A_u + 3B_{1\,u} + 3B_{2\,u} + 3B_{3\,u}$	None	$B_{1\,u}$, $B_{2\,u}$, $B_{3\,u}$
O1	4c	C_s	$2A_g + A_u + B_{1\,g} + 2B_{1\,u} + 2B_{2\,g} + 2B_{2\,u} + B_{3\,g} + 2B_{3\,u}$	A_g, $B_{1\,g}$, $B_{2\,g}$, $B_{3\,g}$	$B_{1\,u}$, $B_{2\,u}$, $B_{3\,u}$
O2	8d	C_1	$3A_g + 3A_u + 3B_{1\,g} + 3B_{1\,u} + 3B_{2\,g} + 3B_{2\,u} + 3B_{3\,g} + 3B_{3\,u}$	A_g, $B_{1\,g}$, $B_{2\,g}$, $B_{3\,g}$	$B_{1\,u}$, $B_{2\,u}$, $B_{3\,u}$

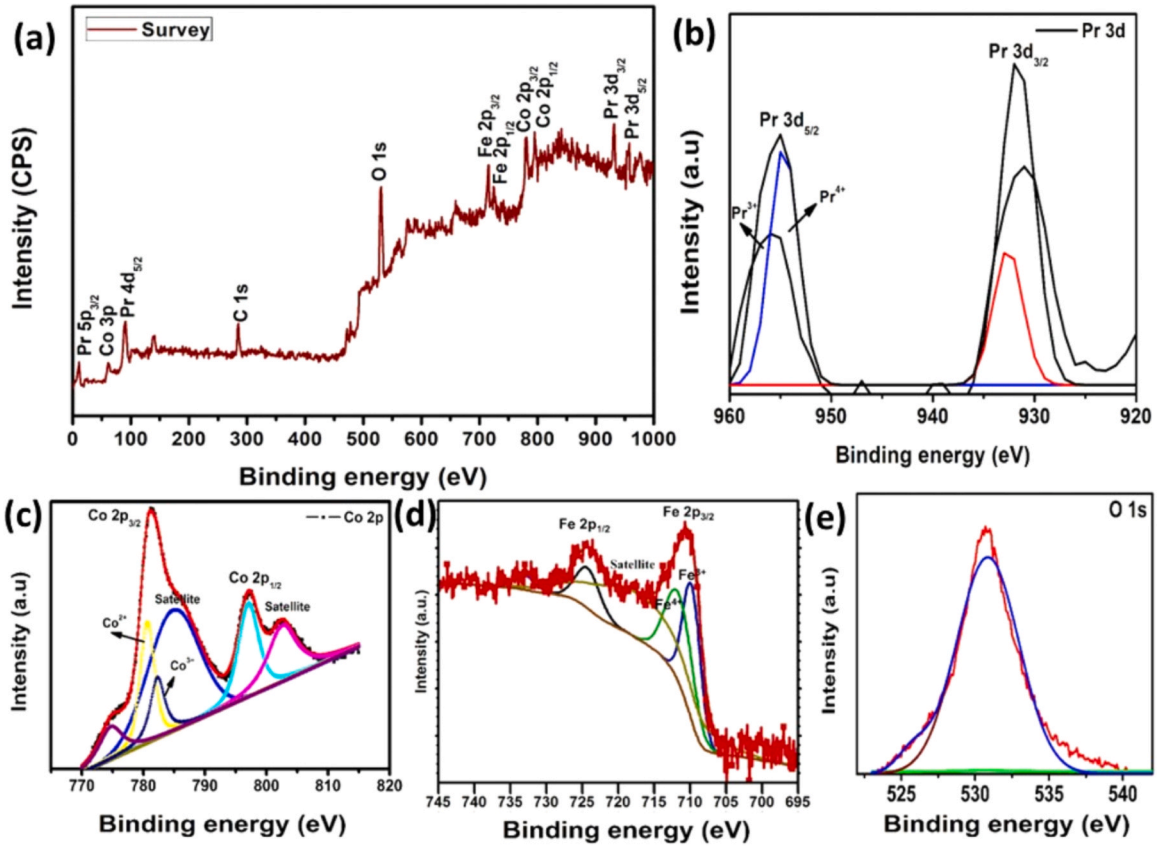

Fig. 5. (a) XPS wide spectrum and deconvolution peaks- (b) Pr 3d, (c) Co 2p, (d) Fe 2p, and (e) O 1 s of the synthesized Pr_2CoFeO_6 compound.

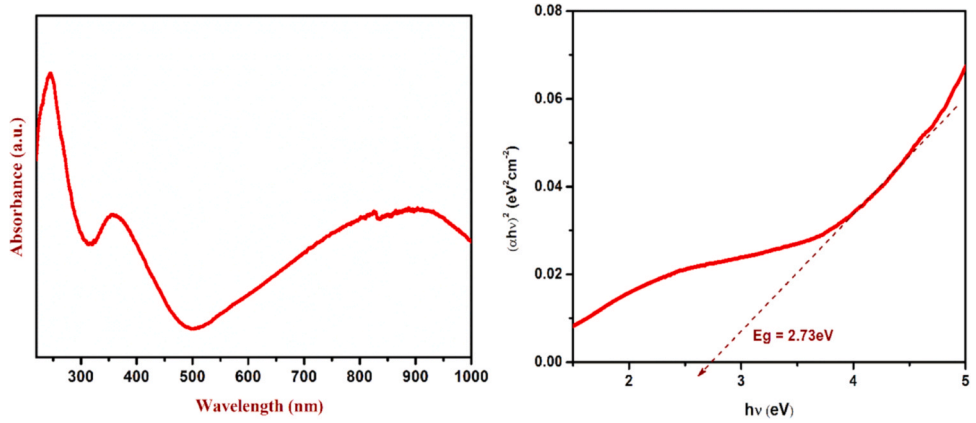

Fig. 6. UV–Vis absorbance spectra (left side) and Tauc plots of $(\alpha h\nu)^2$ versus photon energy ($h\nu$) (right side) of the Pr_2CoFeO_6 compound.

Further, this figure shows ferromagnetic spin alignment ordering. O p states are the main contributors to the valence band, while unoccupied Fe d, Co d, and Pr d states dominate near the bottom of the conduction band. The charge density contour indicates that the Co-O, Fe-O, and Pr-O bonds are mainly ionic. It shows that absorption peaks are detected at 246 and 370 nm. These peaks are due to the band transition from the valence band (O2p) to the conduction band (Fe3d). This is well agreed with our calculated electronic partial density of states and charge density contour.

The magnetic behavior of the Pr_2CoFeO_6 compound at room

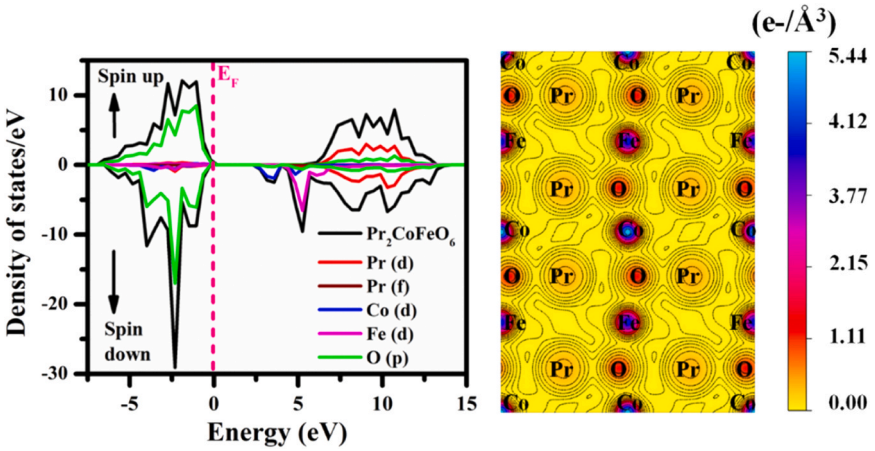

Fig. 7. The electronic density of state and charge density contour of the Pr_2CoFeO_6 compound.

temperature has been analyzed by using the M-H hysteresis curve and a zoomed view of the M-H curve also presented in Fig. 8. From the figure, the M-H hysteresis curve observed retentivity (Mr), coercivity (Hc) and Magnetization (Ms) values are 0.0013 emu, 1322.9 Oe, and 0.0083 emu respectively. The Curie temperature (Tc) is 562 K, which is obtained from the dielectric constant versus temperature in Fig. 12. The maximum dielectric constant at temperature is the Curie temperature. These values show that Pr_2CoFeO_6 exhibited weak ferromagnetic behavior at room temperature due to larger saturation magnetization. This ferromagnetic nature is confirmed by theoretical data. Each atomic contribution of the magnetic moment is presented in Table 4. It shows that Fe and Co atoms make the magnetic moments as 6.34 μ_B for Fe and 1.36 μ_B for Co atoms. The calculated net magnetic moment is ~8 μ_B, which is in good agreement with our experimental (VSM) result. Unexpectedly, we found a weak ferromagnetic nature and it may be uncompensated surface spins associated with large surface areas and its orientation can even exist at room temperature [33].

The magnetization property of materials in a distorted system can be influenced by the structural changes or distortions that occur in the crystal lattice or molecular arrangement. When a material undergoes distortion in its crystal structure, it can impact the magnetic properties of the compound in ways such as magnetic anisotropy, changes in exchange interactions, electronic structure change, magnetic frustration, and domain structure. Understanding the interplay between crystal structure, electronic configuration, and magnetic interactions is crucial for predicting and controlling the magnetization properties of materials in distorted systems. In the present work, it is noticed that the Pr_2CoFeO_6 compound has been formed in a distorted orthorhombic structure. Further, there is a buckling in the position of Pr has also been noted due

Table 4
Projected magnetic moment of the Pr_2CoFeO_6 compound.

Ions	Magnetic moment (μ_B)			
	s	p	d	Total
Pr	0.004	0.008	0.026	0.042
Co	0.008	0.008	1.35	1.365
Fe	0.026	0.024	6.298	6.348
O1	0.04	0.35	0	0.39
O2	0.06	0.42	0	0.48

to the analysis of the Wyckoff position of individual elements, which leads to the strong interplay of magnetic force of attraction between the intermediate layers in the Pr_2CoFeO_6 compound. While considering the ferromagnetic nature of Co and Fe, the intermediate combination Pr-O and Co-Fe layers enhances the anti-spin alignment on their domain and so the net magnetic moments of the prepared compound get reduced.

To further assess the magnetic characteristics of the Pr_2CoFeO_6 compound, we examined an M–T curve under a magnetic field strength of 2k Oe. Analysis of Fig. 9 reveals a decline in magnetization as temperature increases. The temperature-dependent reciprocal magnetic susceptibility (χ^{-1}) is fitted by the Curie-Weiss (CW) law, as expressed by Eq. (4):

$$\chi^{-1}(T) = \frac{T - \theta_p}{C} \tag{4}$$

where C stands for the CW constant and θ_p represents the CW temperature and it can be determined by setting $\chi^{-1}(T) = 0$. Notably, an

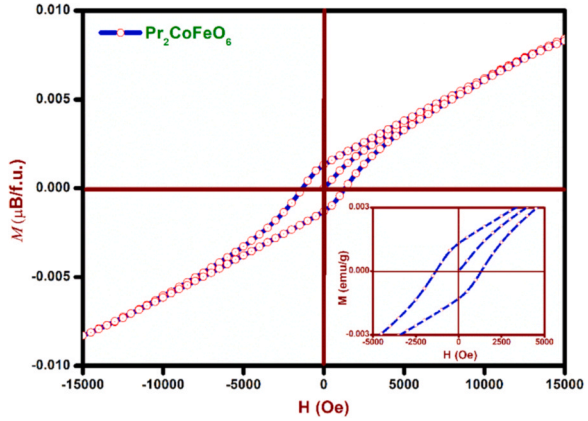

Fig. 8. Room-temperature magnetization curves of the Pr_2CoFeO_6 compound.

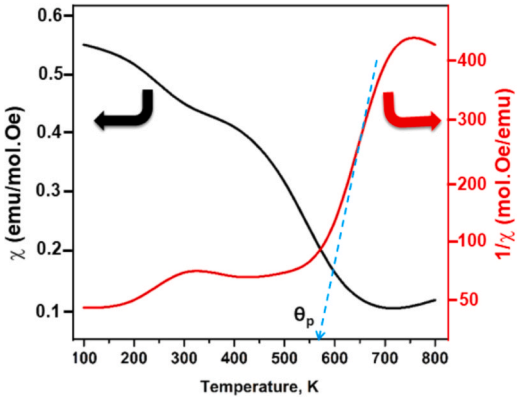

Fig. 9. M–T curve for Pr_2CoFeO_6 compound at 2k Oe field.

extrapolation line intersects at 562 K, indicating the presence of the Curie temperature at this point. Concurrently, the susceptibility and inverse susceptibility values on the y-axis also intersect around 562 K. This suggests that beyond this temperature, the material forfeits its ferromagnetic property, which arises from the interplay between ferromagnetic (FM) and antiferromagnetic (AFM) ordering.

3.6. Photoluminescence

The luminescence behavior of the Pr_2CoFeO_6 has been studied using the photoluminescence spectrum as shown in Fig. 10. This figure observed a broad excitation band at 350 nm, which is due to the transition of 4 f→3d transition and strong excitation peaks observed between 300 nm and 400 nm due to 4 f→3d transition from intra-configuration of Pr^{3+} ions. The PL spectrum consists of four narrow bands, which is characteristic of Pr^{3+} ions in the region of 300 to 400 nm, it is connected with the $^1G_4 \rightarrow {}^1D_0$, $^3H_4 \rightarrow {}^3P_2$, $^3H_4 \rightarrow {}^1D_2$ and $^1I_6 \rightarrow {}^1S_0$ transitions [34], which is due to the crystal-field effects [34,37].

An emission peak is presented at 532 nm due to the transition $^3P_0 \rightarrow {}^3H_5$. The energy level diagram of an emission process in Pr_2CoFeO_6 is schematically provided in Fig. 11, it exhibits the main observed radioactive transitions in the system. The $^1G_4 \rightarrow {}^1D_0$ and $^3H_4 \rightarrow {}^3P_2$ transitions are presented at 332 and 350 nm peaks respectively. Tang Wei et al. [38] recently observed a single blue-green emission from the $^3P_0$ level. The electrons non-radioactively cross over to the $^1D_0$ level as a result of total quenching of the $^3P_2$ level emission due to the tight coupling between the virtual intervalence charge transfer and the $^3P_2$ level at room temperature [39,40]. The figure shows the emission spectra of Pr^{3+} phosphors excited at 350 nm at concentrations ranging. Three manifolds of the $^3P_1 \rightarrow {}^3H_4$ level are responsible for the violet spectral lines detected at 412, 436, and 468 nm. The green spectral lines seen at 532 nm are assigned to the $^3P_0 \rightarrow {}^3H_5$ level, while those shown at 584 and 596 nm are related to the $^3P_0 \rightarrow {}^3H_6$ level manifold [38]. The $^3P_0 \rightarrow {}^3H_5$ transition's green emission appears brighter than the $^3P_1 \rightarrow {}^3H_4$ and $^3P_0 \rightarrow {}^3H_4$ transitions blue emission. This is in contrast to what has been observed in other oxide phosphors such as Ca_2ZnWO_6: Pr^{3+}, $Y_2Mo_4O_{15}$: Pr^{3+}, and LiLaMgWO: Pr^{3+} [41,42], where the emissions due to $^3P_0 \rightarrow {}^3H_5$ transitions are substantially stronger than those owing to $^3P_0 \rightarrow {}^3H_6$. The presence of emission due to the transition from the $^3P_0$ to F levels may indicate that the virtual charge transfer state is positioned in such a way that it is unable to entirely quench this emission in this case. Because multi-phonon relaxation is inefficient, emission from the $^1D_2$ level was more difficult to achieve. The energy gap between the $^3P_0$ and the next lower lying level, the $^1D_2$ is about 4000 cm^{-1} which is larger than the host lattice's low-phonon energy and the strong emission

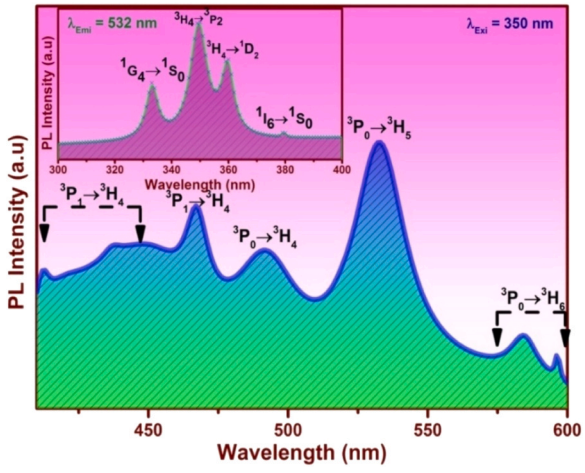

Fig. 10. Photoluminescence emission and excitation spectra of the Pr_2CoFeO_6 compound.

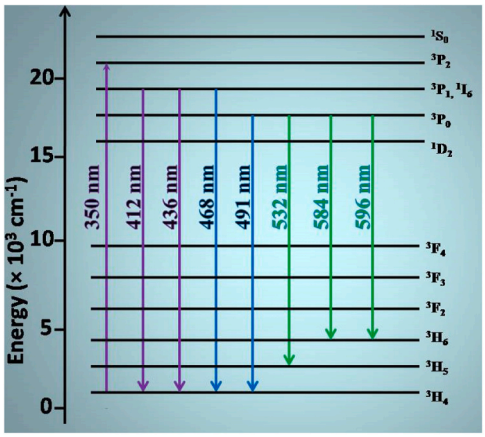

Fig. 11. Energy level diagram of the Pr_2CoFeO_6 compound.

lines are related to Pr^{3+} ion transitions originating from the $^3P_0$ level.

3.7. CIE chromaticity diagram

Using the CIE color chromaticity diagram, we have determined the primary emission color of the Pr_2CoFeO_6 compound with the help of the photoluminescence spectrum. The color matching is necessary to determine the color of the light source. The color mixing functions are listed below and it simulates a certain spectral power (P (λ)) [43].

$$x = \int \bar{x}(\lambda) P(\lambda) d \tag{5}$$

$$y = \int \bar{y}(\lambda) P(\lambda) d \tag{6}$$

$$z = \int \bar{y}(\lambda) P(\lambda) d \tag{7}$$

These x, y, and z indicate tristimulus systems; this is based on the three basic colors: green, yellow, and red. The mixing of these colors reproduces the tone of a certain spectral power density (P). This may be useful to generate a phosphor's chromaticity coordinates of x and y [44].

$$x = \frac{X}{X+Y+Z} \tag{8}$$

$$y = \frac{Y}{X+Y+Z} \tag{9}$$

The CIE Chromaticity system employs some brightness parameters such as Y and other two-color coordinates (x and y) and it defines the mixing of colors, these coordinates correspond to points on the chromaticity diagram. From the CIE diagram, the color triangle is made by mixing three basic colors (blue, green, and red). The calculated CIE Chromaticity diagram of PCFO is presented in Fig. 12, it shows that the color spectrum formed around the color space, and it contains all visible colors. Moreover, it shows that PCFO compounds exhibited blue-green emission as indicated in black dotted points. Computational chromaticity coordinates $x = 0.210$ and $y = 0.252$ for the Pr_2CoFeO_6 compound.

3.8. Dielectric properties

The dielectric properties of the Pr_2CoFeO_6 compound as a function of frequency at different temperatures have been investigated as shown in Fig. 13. The study of dielectric behavior is mainly used to find the polarising nature of the materials. This figure shows that both dielectric constant and loss factor drop with increasing frequency. It indicates that this compound exhibits polar dielectric in nature. At higher

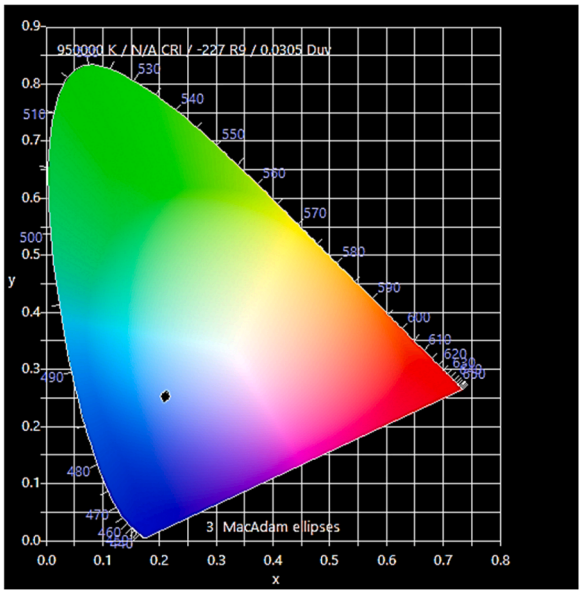

Fig. 12. CIE color phase diagram of the Pr_2CoFeO_6 compound.

temperatures, an accumulation of charge carriers takes place in the grain boundaries and the hopping process requires more energy. Therefore, its permittivity is very high [45,46], whereas this value increases with an increase in the temperature, it does not show any dielectric anomaly in the measured temperature range. This is a similar kind of frequency-dependent on dielectric performance found in many ferroelectric ceramics [47,48]. The dielectric dispersion obtained by lack of invariance translation in free energy barriers of ion diffusion. The dielectric constant exhibits due to the mixing of valence state of Co and Fe ions with two different cations ordered at the B site and this is caused by oxygen vacancies created during sample synthesis and sintering owing to incomplete oxidation. The underlying mechanism is enhanced; the hopping electrons due to mixed valence reduce the resistance in the grains, which causes electrons to reach the grain boundaries and generate dipoles as well as polarization. There are other possibilities where observed relaxation in this system could be related to the electrical inhomogeneity, in which the charge carriers in the grains are imprisoned by the high potential of grain boundary areas. It can be viewed as a very thin capacitor and it has a large dielectric constant. Further, the dielectric constant is nearly constant at the high frequency; it shows a rapid polarisation process with no permanent drastic electronic hopping towards the field direction. The dielectric constant and dielectric loss as a function of temperature at different frequencies have been studied and presented in Fig. 14. The figure shows that The value of dielectric constant and loss is increased with increasing the temperature up to ~500 K for different frequencies and above the 500 K decreases. That maximum of the dielectric constant at a temperature is called Curie temperature. Further, Based on the two-layer model proposed by Maxwell and Wagner, dielectric materials with non-uniform structures are thought to be composed of many well-conducting grains spaced apart by thin, highly resistive boundaries that are poorly conducting between the grains. Assuming that the mechanism of dielectric polarisation is similar to that of the conduction process, the composition-dependent dielectric constant has been explained. As a result, when the sample is subjected to a high voltage, the voltage primarily drops across the grain boundaries, where space charge polarisation is formed [48].

4. Conclusion

The Pr_2CoFeO_6 compound was synthesized and the compound is crystallized in orthorhombic structure with the *Pbnm* space group it was confirmed by the Rietveld refinement XRD analysis. The obtained lattice constant and other parameters are good agreeing with our theoretical and available results. For the Raman spectrum analysis and group theory analysis, the Pr_2CoFeO_6 sample totally presented six Raman modes of vibrations. The UV-DRS spectrum and calculated electronic band structure results found that the band gap value was around 2.73 eV. This compound exhibits weak ferromagnetic order, which is confirmed by the magnetic hysteresis curve and estimated theoretical values. The M–T curve at 2k Oe for Pr_2CoFeO_6 demonstrates a reduction in magnetization with increasing temperature, unveiling a Curie temperature at 562 K, indicative of the ferromagnetic-to-antiferromagnetic (FM-to-AFM) ordering interplay resulting in the loss of ferromagnetic property. Dielectric property results concluded that this compound exhibits a polar dielectric constant. The charge transfer band is attributed to broad bands between 330 and 380 nm in the excitation PL spectrum due to the transition from $^3P_0 \rightarrow {}^3H_5$ to $^3H_6$. The phosphor can be activated by UV radiation from 300 to 400 nm and emits green light at 532 nm. Finally, overall the property of the compound is concluded that the material is very supportive and useful in different applications such as spintronic devices, LED, and data storage devices.

CRediT authorship contribution statement

M DHILIP: Writing – review & editing, Writing – original draft, Validation, Resources, Methodology, Investigation, Data curation, Conceptualization. **Sundaramurthy Rameshkumar:** Writing – review & editing, Writing – original draft, Formal analysis, Data curation, Conceptualization. **Raji Ramesh Kumar:** Writing – review & editing, Writing – original draft, Visualization, Methodology, Investigation, Formal analysis. **Ramachandran Tholkappiyan:** Writing – review &

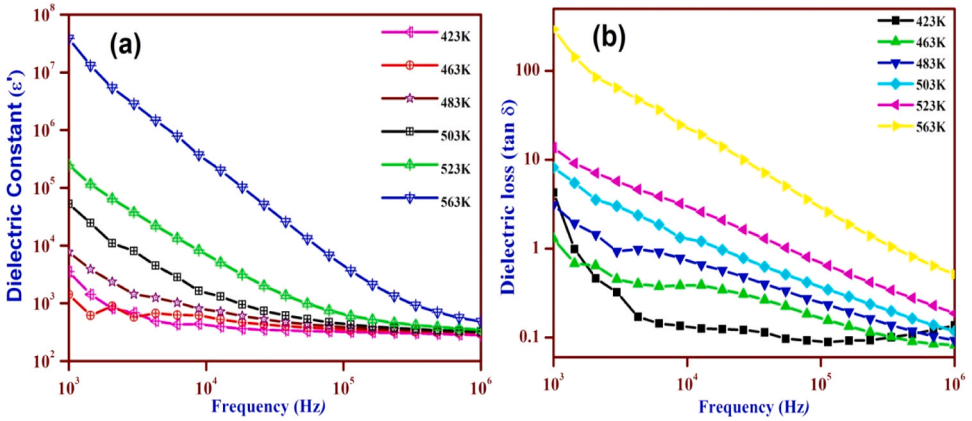

Fig. 13. (a) Frequency dependence of dielectric constant and (b) Frequency dependence of dielectric loss of the Pr_2CoFeO_6 compound.

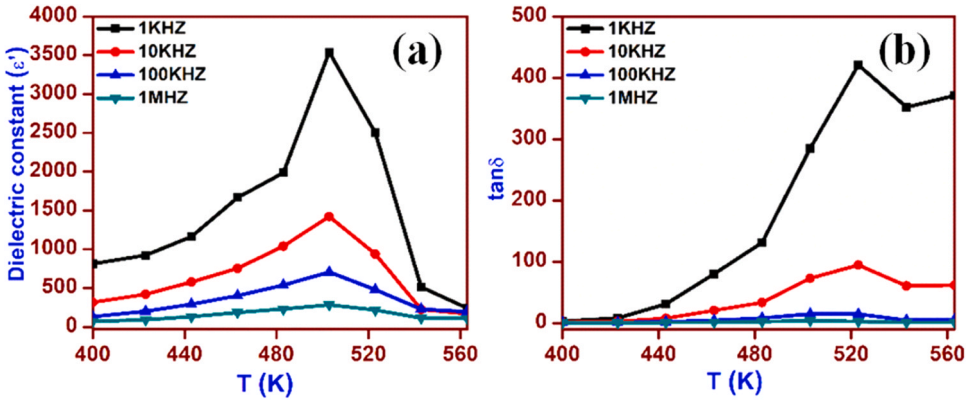

Fig. 14. (a) Dielectric constant and (b) Dielectric loss (tanδ) as a function of temperature at different frequencies of the Pr_2CoFeO_6 compound.

editing, Writing – original draft, Visualization, Methodology, Investigation, Formal analysis, Data curation, Conceptualization. **Punitha J. Stella:** Formal analysis. **Kumar Dr K. Saravana:** Formal analysis. **Anbarasu Dr V.:** Validation, Formal analysis. **Sekar Dr Nandakumar:** Formal analysis. **Sundar Raj F. Regan Maria:** Formal analysis. **Chinnathambi Rajivganthi:** Formal analysis. **A. Ghfar Ayman:** Formal analysis.

Declaration of Competing Interest

The authors declare that they have no known competing financial interests or personal relationships that could have appeared to influence the work reported in this paper.

Data availability

The data that has been used is confidential.

Acknowledgment

The authors gratefully acknowledge the management of SSN College of Engineering, Kalavakkam, Chennai, providing the simulation access.

References

[1] R.K. Raji, M. Muralidharan, T. Ramachandran, et al., Conventional synthesis of perovskite structured $LaTi_xFe_{1-x}O_3$: a comprehensive evaluation on phase formation, opto-magnetic, and dielectric properties,", Int. J. Mater. Res. vol. 112 (9) (2021) 753–765.
[2] K.I. Kobayashi, T. Kimura, H. Sawada, K. Terakura, Y. Tokura, Nature 395 (1998) 677–680.
[3] Tanmoy Maiti, Mandvi Saxena, Pinku Roy, Double perovskite ($Sr_2B'B''O_6$) oxides for high-temperature thermoelectric power generation - A review, J. Mater. Res. 34 (2019) 107–125.
[4] Nurxat Nuraje, Kai Su, Perovskite ferroelectric nanomaterials, Nanoscale 5 (19) (2013) 8752–8780.
[5] R.R. Kumar, T. Ramachandran, K. Natarajan, M. Muralidharan, F. Hamed, V. Kurapati, Fraction of rare-earth (Sm/Nd)-lanthanum ferrite-based perovskite ferroelectric and magnetic nanopowders, Article ID 1694, J. Electron. Mater. vol. 48 (3) (2019). Article ID 1694.
[6] R.K. Raji, M. Muralidharan, T. Ramachandran, et al., Dualphase formation in $LaFeO_3$ upon doping of rare-earth Dy^{3+}:struct–opto–dielectric–magnetic characteristics,", J. Mater. Sci.: Mater. Electron. vol. 33 (2) (2022) 10626–10644.
[7] R. Tholkappiyan, T. Thiemann, F. Hamed, Phase evolution and magnetic properties of $Dy_3Fe_{5+x}O_{12-x}$ nanocrystalline powders: a choice of fuel approach,", Mater. Chem. Phys. vol. 240 (2020) 122138.
[8] T. Ramachandran, A.-H.I. Mourad, R.K. Raji, et al., KOH mediated hydrothermally synthesized hexagonal-$CoMn_2O_4$ for energy storage supercapacitor applications, Int. J. Energy Res. 46 (12) (2022) 16823–16838, https://doi.org/10.1002/er.8350.
[9] Yedluri Anil Kumar, Ganesh Koyyada, Tholkappiyan Ramachandran, Jae Hong Kim, H.H. Hegazy, Sangeeta Singh, Md Moniruzzaman, Recent advancement in quantum dot-based materials for energy storage applications: a review, Dalton Trans. 52 (2023) 8580–8600, https://doi.org/10.1039/D3DT00325F.
[10] R. Tholkappiyan, K. Vishista, Tuning the composition and magnetostructure of dysprosium iron garnets by Co-substitution: an XRD, FT–IR, XPS and VSM study, Appl. Surf. Sci. 351 (2015) 1016–1024, https://doi.org/10.1016/j.apsusc.2015.05.193.
[11] Towfiq Ahmed, Aiping Chen, Dmitry A. Yarotski, Stuart A. Trugman, Quanxi Jia, Jian-Xin Zhu, APL Mater. 5 (2017) 035601.
[12] Jasnamol Pezhumkattil Palakkal, P.Neenu Lekshmi, Senoy Thomas, K.G. Suresh, Manoj Raama Varma, RSC Adv. 5 (2015) 105531–105536.
[13] Manish Kumar, Brijmohan Prajapati, Abhishek Singh, Shiv Kumar, Arvind Kumar, Srishti Mittal, Aditya, Chem. Phys. 532 (2020) 110688.
[14] L.Y. Wang, Q. Li, Y.Y. Gong, D.H. Wang, Q.Q. Cao, Y.W. Du, The positive and negative magnetodielectric effect in double perovskite Pr_2CoMnO_6, J. Am. Ceram. Soc. 97 (2014) 2024–2026.
[15] Tholkappiyan Ramachandran, Fathalla Hamed, Ramesh Kumar Raji, Sanjit Manohar Majhi, Debabrata Barik, Yedluri Anil Kumar, R.O.M.U. Jauhar, M. P. Pachamuthu, L. Vijayalakshmi, Sabah Ansar, Enhancing asymmetric supercapacitor performance with $NiCo_2O_4$–NiO hybrid electrode fabrication, J. Phys. Chem. Solid. 180 (2023) 111467, https://doi.org/10.1016/j.jpcs.2023.111467.
[16] Kulurumotlakatla Dasha Kumar, Yedluri Anil Kumar, Tholkappiyan Ramachandran, A.Abdullah Al-Kahtani, MyungChang Kang, Cactus-like Ni-Co/$CoMn_2O_4$ composites on Ni foam: unveiling the potential for advanced electrochemical materials for pseudocapacitors, Mater. Sci. Eng. B 296 (2023) 116715, https://doi.org/10.1016/j.mseb.2023.116715.
[17] R. Tholkappiyan, Fathalla Hamed, K. Vishista, Effect of annealing conditions on the struct-optical properties of $ZnFe_{1.96}La_{0.04}O_4$ nanoparticles, Adv. Mater. Lett. 7 (12) (2016) 971–978, https://doi.org/10.5185/amlett.2016.6387.
[18] Moumita Das, Prabhat Mandal, Nonlinear magnetodielectric and magnetocaloric properties of double perovskite Ho_2FeCoO_6, Phys. B: Condens. Matter 571 (2019) 32–35.
[19] G.R. Haripriya, R. Pradheesh, K. Sethupathi, V. Sankaranarayanan, The order of magnetic phase transitions in disordered double perovskite oxides Sm_2FeCoO_6 and Dy_2FeCoO_6, AIP Adv. 8 (10) (2018) 101340.
[20] Arkadeb Pal, Surajit Ghosh, Amish G. Joshi, Shiv Kumar, Swapnil Patil, Prince K. Gupta, Prajyoti Singh, et al., Investigation of multi-mode spin–phonon coupling and local B-site disorder in Pr_2CoFeO_6 by Raman spectroscopy and correlation with its electronic structure by XPS and XAS studies, J. Phys.: Condens. Matter 31 (27) (2019) 275802.
[21] Hao Wu, Xiao-Lei Shi, Wei-Di Liu, Meng Li, Han Gao, Wei Zhou, Zongping Shao, Yifeng Wang, Qingfeng Liu, Zhi-Gang Chen, Double perovskite Pr_2CoFeO_6 thermoelectric oxide: Roles of Sr-doping and Micro/nanostructuring, Chem. Eng. J. 425 (2021) 130668.
[22] H.M. Rietveld, A Profile Refinement Method for Nuclear and Magnetic Structures, J. Appl. Crystallogr. 2 (1969) 65–71.
[23] D. Vijayalakshmi, Tholkappiyan Ramachandran, G. Jaiganesh, G. Kalpana, Fathalla Hamed, Unveiling the Robust Struct-Electromagnetic Characteristics of $CdAB_2$ Chalcopyrite (A = Cr, Mn, Fe; B = P, As): A Comprehensive Ab-Initio Study, Adv. Condens. Matter Phys. (2023) 1754324, https://doi.org/10.1155/2023/1754324.
[24] John P. Perdew, Kieron Burke, Matthias Ernzerhof, Generalized gradient approximation made simple, Phys. Rev. Lett. 77 (18) (1996) 3865.
[25] Blöchl, E. Peter, Projector augmented-wave method, Phys. Rev. B 50 (24) (1994) 17953.
[26] H.J. Monkhorst, J.D. Pack, Special points for Brillouin-zone integrations, Phys. Rev. B 13 (12) (1976) 5188–5192.
[27] Tuan V. Vu, A.A. Lavrentyev, B.V. Gabrelian, O.V. Parasyuk, V.A. Ocheretova, O. Y. Khyzhun, Electronic structure and optical properties of $Ag_2HgSnSe_4$: First-principles DFT calculations and X-ray spectroscopy studies, J. Alloy. Compd. 732 (2018) 372–384.
[28] Tuan V. Vu, A.A. Lavrentyev, B.V. Gabrelian, V.A. Ocheretova, O.V. Parasyuk, O. Y. Khyzhun, Particular features of the electronic structure and optical properties of Ag_2PbGeS_4 as evidenced from first-principles DFT calculations and XPS studies, Mater. Chem. Phys. 208 (2018) 268–280.
[29] Tuan V. Vu, A.A. Lavrentyev, B.V. Gabrelian, Hien D. Tong, V.A. Tkach, O. V. Parasyuk, O.Y. Khyzhun, A theoretical and experimental study of the valence-

band electronic structure and optical constants of quaternary copper mercury tin sulfide, Cu_2HgSnS_4, a potential material for optoelectronics and solar cells, Opt. Mater. 96 (2019) 109296.
[30] B.V. Gabrelian, A.A. Lavrentyev, Tuan V. Vu, K.F. Kalmykova, L.N. Ananchenko, V. A. Tkach, O.V. Parasyuk, O.Y. Khyzhun, Valence-band electronic structure and main optical properties of $Cu_2HgGeTe_4$: Theoretical simulation within a DFT framework and experimental XPS study, Mater. Today Commun. 23 (2020) 100828.
[31] M.T. Anderson, K.B. Greenwood, G.A. Taylor, K.R. Poeppelmeier, Prog. Solid State Chem. 22 (1993) 197.
[32] P. Kumar, R. Singh, P.C. Pandey, J. Appl. Phys. 123 (2018) 054502.
[33] Shidaling Matteppanavar, Sudhindra Rayaprol, Anupama A.V. BasavarajAngadi, Balaram Sahoo, Origin of room temperature weak-ferromagnetism in antiferromagnetic Pb(Fe2/3W1/3)O3 ceramic, Ceram. Int. 41 (2015) 11680–11686.
[34] C.D.S. Brites, K. Fiaczyk, J.F.C.B. Ramalho, M. Sójka, L.D. Carlos, E. Zych, Widening the temperature range of luminescent thermometers through the intra- and interconfigurational transitions of Pr^{3+}, Adv. Opt. Mater. 6 (2018) 1701318.
[35] X.C. Jiang, W.M. Chen, C.Y. Chen, S.X. Xiong, A.B. Yu, Nanoscale Res. Lett. 6 (2011) 32.
[36] W. Ran, H.M. Noh, S.H. Park, B.K. Moon, J.H. Jeong, J.H. Kim, J. Shi, Sci. Rep. 8 (2018) 5936.
[37] M. Runowski, A. Shyichuk, A. Tymiński, T. Grzyb, V. Lavín, S. Lis, Multifunctional optical sensors for nanomanometry and nanothermometry: high-pressure and hightemperature upconversion luminescence of lanthanide-doped phosphates—lapo$_4$/ YPO_4:Yb^{3+}, Tm^{3+}, ACS Appl. Mater. Interfaces 10 (2018) 17269–17279.
[38] Tang Wei, Ni Haiyong, Zhang Qiuhong, Ding Jianhong, Novel optical temperature sensor based on emission in Pr^{3+} doped ferroelectric $Ba_{0.7}Sr_{0.3}TiO_3$, RSC Adv. 8 (2018) 23996.
[39] P. Boutinaud, E. Pinel, M. Dubois, A.P. Vink, R. Mahiou, J. Lumin. 111 (2005) 69.
[40] Guilin Yan, Wentao Zhang, Yi Huang, Peicong Zhang, Junfeng Li, J. Mater. Sci.: Mater. Electron. 30 (2019) 14589–14599.
[41] K.V. Dabre, S.J. Dhoble, Synthesis and photoluminescence properties of Eu3+, Sm3 + and Pr3+ doped Ca2ZnWO6 phosphors for phosphor converted LED, J. Luminesc. 150 (2014) 55–58.
[42] Jiawen Wang, Nan Chen, Junyi Li, Qingyang Feng, Ruoshan Lei, Huanping Wang, Shiqing Xu, J. Lumin. 238 (2021) 11824.
[43] K. Ji Eon, S. Park, S. Young Park, Realizing molecular pixelsystem for full-color fluorescence reproduction: RGB-emittingmolecular mixture free from energy transfer crosstalk, J. Am. Chem. Soc. 135 (2013) 11239–11246.
[44] A.Juan Enrique, P.J. Pardo, H. Sánchez, Á. Luis Pérez, M. IsabelSuero, A low-cost real color picker based on arduino, Sensors 14 (2014) 11943–11956.
[45] Shidaling Matteppanavar, Sudhindra Rayaprol, AnupamaA.V. BasavarajAngadi, Balaram Sahoo, Origin of room temperature weak-ferromagnetism in antiferromagnetic Pb(Fe2/3W1/3)O3 ceramic, Ceram. Int. 41 (2015) 11680–11686.
[46] Ramesh Kumar Raji, Tholkappiyan Ramachandran, M. Muralidharan, R. Suriakarthick, M. Dhilip, A. Raja, Vishista Kurapati, Fathalla Hamed, P. Ramasamy, Abdel-Hamid I. Mourad, Twitching the inherent properties: the impact of transition metal Mn-doped on $LaFeO_3$ based perovskite materials, J. Mater. Sci.: Mater. Electron. 32 (2021) 25528–25544.
[47] Nibedita Das, R. Singh, A. Das, Laxmi C. Gupta, Ashok K. Ganguli, Structural, magnetic and dielectric properties of a new double perovskite Pr_2CoTiO_6, J. Solid State Chem. 253 (2017) 355–359.
[48] Ramesh Kumar Raji, Vishista Kurapati, Tholkappiyan Ramachandran, M. Muralidharan, R. Suriakarthick, M. Dhilip, Fathalla Hamed, Tweaking the red emission, magneto, and dielectrical properties of perovskite type-$LaFeO_3$ in the presence of Co substitution, J. Mater. Sci.: Mater. Electron. 31 (2020) 7998–8014.